

# X-Ray Reflectivity and Grazing Incidence Diffraction Studies of Interaction between Human Adhesion/Growth-Regulatory Galectin-1 and DPPE–GM1 Lipid Monolayer at an Air/Water Interface

J. Majewski<sup>1</sup>, S. André<sup>2</sup>, E. Jones<sup>3</sup>, E. Chi<sup>3</sup>, and H.-J. Gabius<sup>2\*</sup>

<sup>1</sup>Manuel Lujan Jr. Neutron Scattering Center, Los Alamos Neutron Science Center,  
Los Alamos National Laboratory, Los Alamos, NM, USA

<sup>2</sup>Institute of Physiological Chemistry, Faculty of Veterinary Medicine, Ludwig-Maximilians-University Munich,  
Vetärstr. 13, 80539 München, Germany; E-mail: gabius@tiph.vetmed.uni-muenchen.de; gabius@lectins.de

<sup>3</sup>Department of Chemical and Biological Engineering, Center for Biomedical Engineering,  
University of New Mexico, Albuquerque, NM, USA

Received October 26, 2014

Revision received April 14, 2015

**Abstract**—The specific interaction of ganglioside GM1 with the homodimeric (prototype) endogenous lectin galectin-1 triggers growth regulation in tumor and activated effector T cells. This proven biorelevance directed interest to studying association of the lectin to a model surface, i.e. a 1,2-dihexadecanoyl-*sn*-glycero-3-phosphoethanolamine/ganglioside GM1 (80 : 20 mol%) monolayer, at a bioeffective concentration. Surface expansion by the lectin insertion was detected at a surface pressure of 20 mN/m. On combining the methods of grazing incidence X-ray diffraction and X-ray reflectivity, a transient decrease in lipid-ordered phase of the monolayer was observed. The measured electron density distribution indicated that galectin-1 is oriented with its long axis in the surface plane, ideal for *cis*-crosslinking. The data reveal a conspicuous difference to the way the pentameric lectin part of the cholera toxin, another GM1-specific lectin, is bound to the monolayer. They also encourage further efforts to monitor effects of structurally different members of the galectin family such as the functionally antagonistic chimera-type galectin-3.

**DOI:** 10.1134/S0006297915070135

**Key words:** agglutinin, Bragg peaks, ganglioside, lectin, X-ray diffraction/reflectivity

Cell surface gangliosides are receiving increasing attention due to their emerging spectrum of functions, for example as constituents of microdomains within the plasma membrane and as contact site for carbohydrate receptors (lectins) such as the pentameric lectin part of the cholera toxin (Ctx) [1–4]. Recently, ganglioside GM1, the Ctx counter-receptor, has been identified as a physiological target for human adhesion/growth-regulatory galectins, a family of tissue lectins that share the  $\beta$ -sandwich fold and a sequence signature with a central

tryptophan residue for ligand contact [5–8]. The pentasaccharide of GM1 is a branched structure (Fig. 1b). Binding to galectins involves both branches, the lectin accommodating a conformer of the glycan different from the Ctx-bound structure [9, 10]. To quantitate stability of complexes with glycans, atomic force microscopy was applied. The dissociation kinetics under force for complexes of the prototype (homodimeric) galectin-1 (Gal-1) and common ligands (lactose, asialofetuin) is compatible with a role in transient *trans*-bridging and *cis*-crosslinking [11]. Functionally, Gal-1 exerts growth control via GM1 binding on human neuroblastoma (SK-N-MC) cells and on activated T effector cells *in vitro* [12–16]. In both cases, GM1 is made available enzymatically by a sialidase from its precursor GD1a. As reported for bacterial AB<sub>5</sub> toxins and their entry into cells [17, 18], association with the ganglioside is also involved in rapid

**Abbreviations:** Ctx, cholera toxin pentamer; DPPE, 1,2-dihexadecanoyl-*sn*-glycero-3-phosphoethanolamine; Gal, galectin; GIXD, grazing incidence X-ray diffraction; LC phase, lipid-condensed phase; PSD, position-sensitive detector; XR, X-ray reflectivity.

\* To whom correspondence should be addressed.

internalization of Gal-1 measured in T leukemic (Jurkat) cells [19]. Interestingly, pentameric GM1-specific bacterial lectins also appear to ameliorate autoimmune disorders in animal models [20–22]. However, membrane reactivity to Ctx and the human lectin will not necessarily cause the same post-binding mechanisms: only the human lectin is a growth regulator for the neuroblastoma cells [23]. This functional difference gives reason to assume that topological aspects of the complexes are different, prompting us to initiate the analysis of galectin binding to a GM1-containing model surface at a bioeffective concentration.

In addition to the impact on proliferation as well as cellular uptake and routing, the study of Gal-1 association to the surface of trypsinized erythrocytes had revealed an alteration of membrane fluidity and osmofragility [24]. This effect may depend on a change in the quaternary structure of Gal-1 upon entering the hydrophobic environment. Of note, in an aprotic solvent (i.e. dimethyl sulfoxide) the lectin had been demonstrated to form a dimer of two homodimers with cylindrical shape [25]. Collectively, this evidence led us to start our study with examining the possibility of an insertion of this potent effector protein into a lipid monolayer.

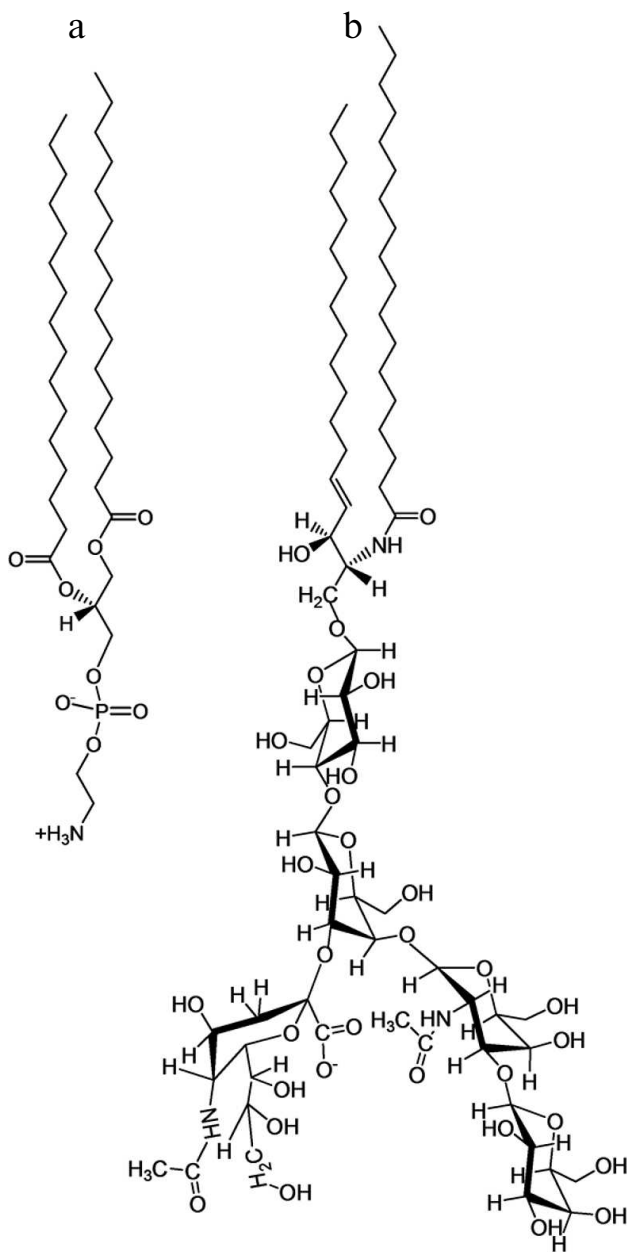


**Fig. 1.** Structures of the (glyco)sphingolipids DPPE (a) and GM1 (b), the constituents of the lipid film.

## MATERIALS AND METHODS

**Materials.** 1,2-Dihexadecanoyl-*sn*-glycero-3-phosphoethanolamine (DPPE) and ganglioside GM1 (brain, ovine-ammonium salt, powder) were purchased from Avanti Polar Lipids (USA) and used without further purification (for structures, see Fig. 1). Stock solutions of each (glyco)sphingolipid (~5 mg/ml) were first prepared in chloroform containing 9% (v/v) methanol and 1% (v/v) water. Lipid monolayer-spreading solutions (0.3 mg/ml) containing 80 mol% DPPE and 20 mol% GM1 (8 : 2 DPPE/GM1) were then prepared and stored at –20°C in glass vials until use. Human Gal-1 was obtained by recombinant production, purified by affinity chromatography as crucial step, and rigorously controlled for purity (by two-dimensional gel electrophoresis and mass-spectrometric fingerprinting) and for bioactivity (by hemagglutination and assays measuring growth inhibition) [12, 26–28].

**Constant-pressure insertion assay with lipid monolayer.** Assays to determine insertion of the protein into the monolayer at the air/buffer interface under constant surface pressure were carried out in a Langmuir trough at the BW1 (undulator) beam line of the HASYLAB synchrotron source (Germany) as described previously [29]. The scheme of the experimental setup of the constant-pressure protein insertion assay and its course is shown in Fig. 2. The temperature-controlled trough at the dedicated liquid surface diffractometer was equipped with a Wilhelmy plate balance that measures surface pressure at the air/buffer interface and a movable hydrophobic Teflon barrier that controls the trough surface area. The trough was first filled with approximately 240 ml of subphase buffer (20 mM phosphate-buffered saline (PBS) at pH 7.2 containing 16.2 mM Na<sub>2</sub>HPO<sub>4</sub>, 4 mM KH<sub>2</sub>PO<sub>4</sub>, 154 mM NaCl, and 1% NaN<sub>3</sub>) at 20°C. A solution of mixed lipids (8 : 2 DPPE/GM1; 90 : 9 : 1 chloroform–methanol–water) was then spread at the air/buffer interface. The system was allowed to equilibrate for 15 min to ensure complete evaporation of organic solvent, after which the lipid monolayer was compressed to a surface pressure of 20 mN/m, and this pressure was kept

constant for the remainder of the experiment via a feedback loop (Fig. 2a). X-Ray scattering data were then collected on the lipid film at 20 mN/m and 20°C (described in more detail below). Having herewith defined the control value, measurements were done in the presence of Gal-1. An aliquot of Gal-1-containing solution (5 mg dissolved in PBS) was injected into the buffer subphase of the trough and allowed to equilibrate with the lipid monolayer (Fig. 2b). The galectin concentration in the trough subphase was approximately 21 µg/ml. Since the surface pressure of lipid monolayer was kept constant, insertion of Gal-1 into the lipid monolayer will result in an expansion of the surface area (Fig. 2c). Thus, the detectable increase in monolayer surface area is taken as a measure of productive galectin–membrane interactions. X-Ray scattering data were taken 5 h ( $t_1$ ) and 13 h ( $t_2$ ) after injecting Gal-1-containing solution.

**X-Ray scattering measurements.** To elucidate the molecular-scale structure of the Gal-1–lipid monolayer film, complementary grazing incidence X-ray diffraction (GIXD) and X-ray reflectivity (XR) data were collected before (lipid membrane alone) and two time points ( $t_1$  and  $t_2$ ) after bringing in Gal-1 into the solution underneath the lipid monolayer. The X-ray beam directed to the sample has a wavelength ( $\lambda$ ) of  $1.30 \pm 0.02$  Å (9510 eV) and a power of about 0.3 mW. To reduce scattering background and to minimize oxidative damage to the protein–lipid film by the X-ray beam, the trough container was purged for 30–40 min with helium. As an additional precaution against damage by radiation, the trough was moved by 0.025 mm in the horizontal direction after every step during the GIXD scans and by 2 mm during the XR scans.

GIXD measurements provide structural in-plane (i.e. in the plane of the monolayer) information on the crystalline diffracting portion of the film. In general, the lipid-condensed (LC) phase in Langmuir monolayers can be described as 2D powers with 2D crystallites that are azimuthally and randomly oriented on the subphase surface. The reciprocal space of GIXD patterns from the crystalline portion of the monolayer arises from a 2D array of Bragg rods, which extend parallel to the vertical component,  $q_z$ , of the scattering vector  $q$  [30, 31]. To maximize surface sensitivity for the GIXD measurements, the monochromatic X-ray beam was adjusted to meet the surface at an incident grazing angle of 0.11°, which is 85% of the critical angle for total external reflection [32]. The dimensions of the footprint of the incoming X-ray beam on the liquid surface were approximately  $2 \times 50$  mm<sup>2</sup>. Diffracted intensities were collected using a one-dimensional position-sensitive detector (PSD, OEM-100-M; Braun, Germany) as a function of the vertical scattering angle and with a measuring window of  $\Delta q_z \approx 0.9$  Å<sup>-1</sup>. A Soller collimator was mounted in front of the PSD, which gave a horizontal resolution of the detector of  $\Delta q_{xy} = 0.0084$  Å<sup>-1</sup>. The scattered intensity was

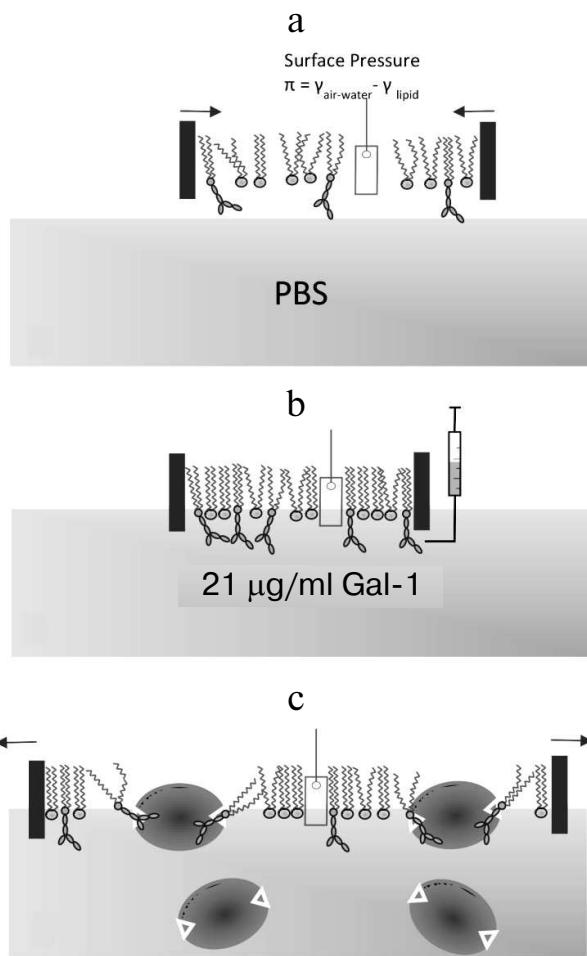


**Fig. 2.** a) Compression of lipid monolayer to 20 mN/m. A Wilhelmy plate surface pressure sensor was used to measure the surface pressure ( $\pi$ ) of the lipid monolayer, which is related to the surface tension ( $\gamma$ ) at the air/water interface. b) Injection of Gal-1 into the subphase. The protein was brought into the subphase underneath the barriers using an L-shaped syringe needle to minimize disturbances to the lipid monolayer. The final Gal-1 concentration has been shown to be bioeffective in *in vitro* assays in GM1-dependent cell growth assays (effector T and neuroblastoma cells). c) Expansion of the lipid monolayer due to the insertion of Gal-1. The homodimeric lectin with its two binding sites is drawn to scale in shape, assuming loading of both contact sites with ligand. Monolayer surface area was recorded and the area expansion was calculated as  $\Delta A/A = (A - A_i)/A_i$ , where  $A$  is the surface area at time  $t$  and  $A_i$  is the surface area of the monolayer when first compressed to 20 mN/m.

measured by scanning over a range of the horizontal scattering vector component:

$$q_{xy} \approx (4\pi/\lambda) \cdot \sin(2\theta_{xy}/2),$$

where  $2\theta_{xy}$  is the angle between the incident and diffracted beam projected onto the horizontal plane, and  $\lambda$  is the wavelength of the X-ray beam. Such a scan, integrated over the whole window of the PSD, yields the Bragg peaks. Simultaneously, the scattered intensity recorded in chan-

nels along the PSD but integrated over the scattering vector in the horizontal plane across a Bragg peak produces  $q_z$ -resolved scans, called Bragg rod profiles. The intensity distribution along a Bragg rod can be analyzed in terms of a model of the molecular conformation, orientation, and packing, to yield information on the direction and magnitude of the molecular tilt in the crystalline part of the amphiphilic film. In this study, lipid tails were modeled by a cylinder of constant electron distribution. Adjustable parameters, under these conditions, were the tilt angle of the cylinder from vertical, the lateral tilt direction, the length,  $L_c$ , of the cylinder (i.e. the length of the part of the molecule which scatters coherently), and the vertical root-mean-square displacement,  $\sigma_z$  (Debye–Waller factor), in the crystallites. Analysis of the Bragg peaks yields  $d$ -spacing and coherence length (i.e. average size) of the 2D crystallites in the film at the air/buffer interface.

While GIXD measurements afford structural information on the in-plane crystalline portion of the film, XR measurements yield information about the out-of-plane (vertical) monolayer structure, laterally averaged over both crystalline and amorphous portions [33, 34]. For XR measurements, an additional slit is used to exclude diffuse scattered background around the reflected beam. This slit, together with a scintillation detector having a thin vertical measuring window ( $\Delta q_z \approx 0.02 \text{ \AA}^{-1}$ ), is mounted on an elevator connected to a diffractometer arm, which is pivoted around a vertical axis through the sample center. Detailed information on electron density variation in the vertical direction, laterally averaged over both the ordered and disordered parts of the film, can be obtained from the deviation of the measured specular XR from Fresnel's law [30, 31].

## RESULTS

### Insertion of Gal-1 into DPPE–GM1 monolayer.

During the lipid monolayer insertion assay, the monolayer surface area was recorded, the change determined, and the percentage of area expansion ( $\% \Delta A/A$ ) calculated using the equation:

$$\% \Delta A/A = 100 \cdot (A - A_i)/A_i,$$

where  $A_i$  is the (initial) trough area of the monolayer at 20 mN/m and 20°C before injecting Gal-1-containing solution and  $A$  is the trough area at time  $t$  after applying the protein (Fig. 2). The isotherm and insertion data are summarized in Fig. 3. The data reveal integration of the lectin, at a concentration effective for GM1-dependent cell growth regulation [12, 13], into the lipid monolayer, as schematically indicated in Fig. 2c.

As shown in Fig. 3b, Gal-1 inserted into the monolayer immediately after starting the experiment by injection of protein-containing solution into the buffer sub-

phase and steadily continued to do so during the period of 7 h. The area per molecule shown here reflects the average area per lipid molecule, accounting for both ordered (LC) and disordered (liquid-expanded) phases. Of note, the “bilayer-equivalent surface pressure”, i.e. the pressure at which the packing density of the monolayer lipid mimics that in a lipid bilayer, has been reported to be in the range of 30–33 mN/m [35]. Thus, an insertion assay at a constant surface pressure of 30 mN/m was first carried out. Because no lectin insertion into the lipid monolayer was yet observed at this pressure, the surface pressure was lowered to 20 mN/m.

**Structure of Gal-1–lipid monolayer film at air/buffer interface.** By combining the methods of GIXD and XR, the in-plane and out-of-plane structures of the lipid film and location of the lectin at the lipid film interface were elucidated. First, a contour plot of the GIXD data for the monolayer, with both  $q_{xy}$  and  $q_z$  resolved, is presented (Fig. 4). Very similarly shaped contour plots for the

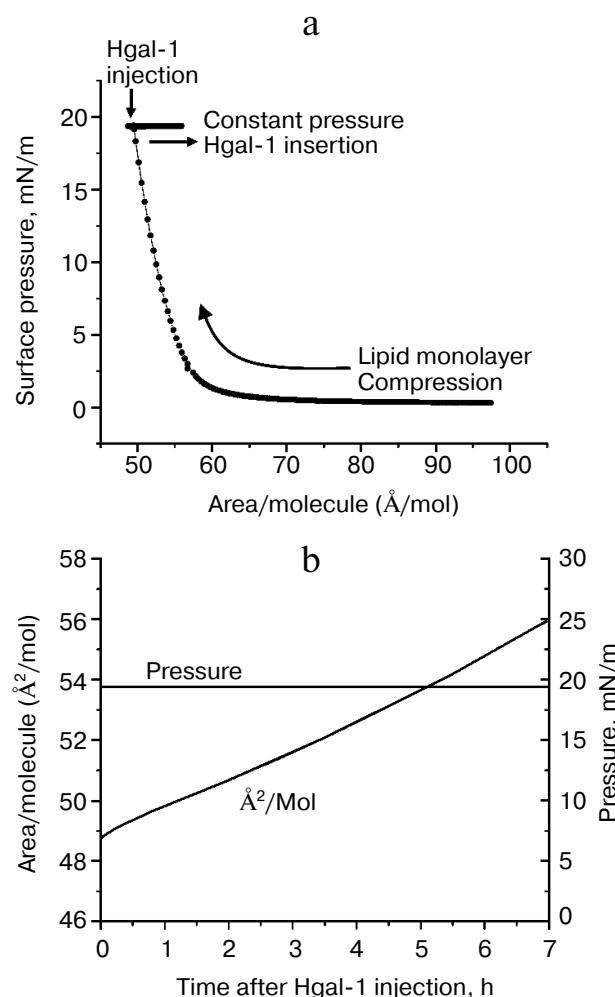
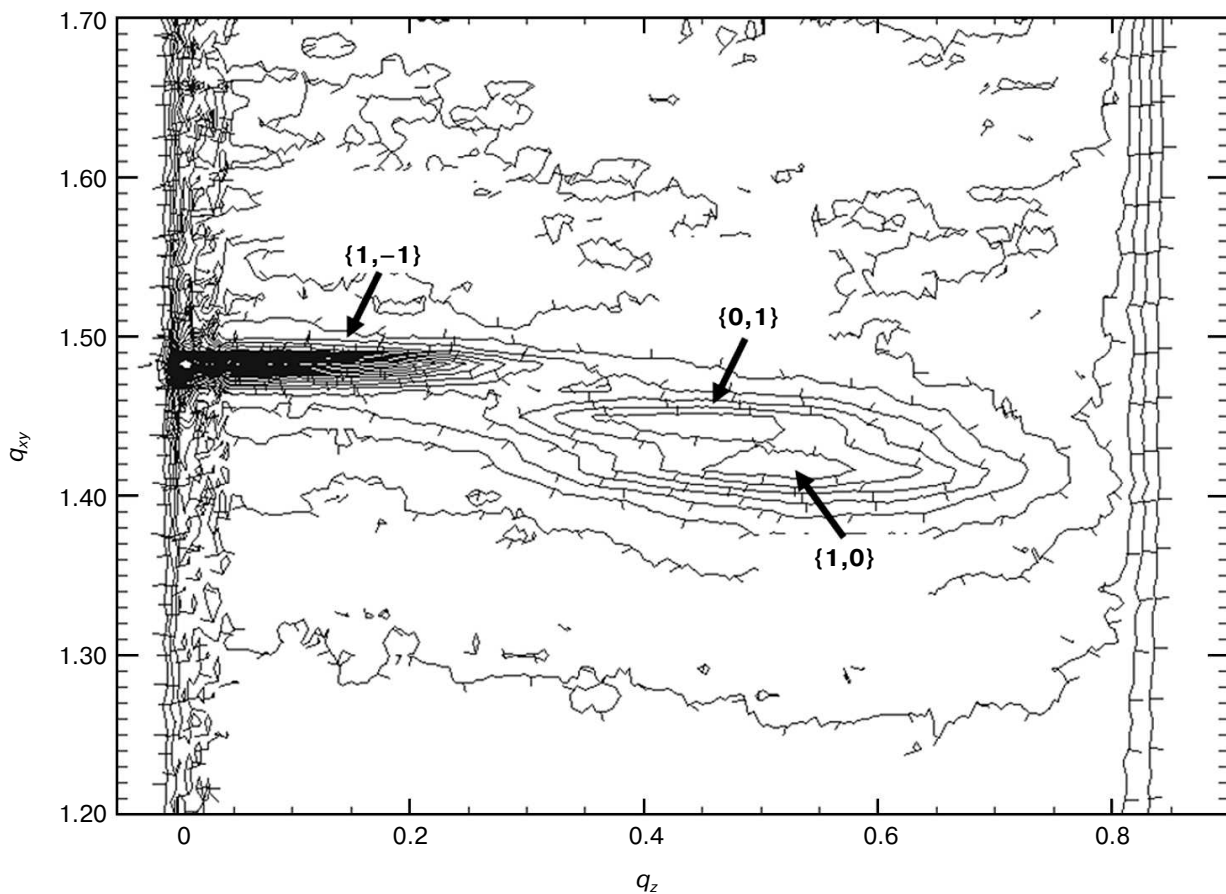


Fig. 3. Isotherm (a) and insertion (b) of Gal-1 into the DPPE–GM1 monolayer held at 20 mN/m at 20°C.



**Fig. 4.** Reciprocal space contour plot,  $I(q_{xy}, q_z)$ , of a DPPE-GM1 monolayer at 20 mN/m and 20°C.

monolayer after lectin insertion were obtained, although absolute intensities of the plots differed (data not shown). GIXD data projected on the  $q_{xy}$  and on  $q_z$  axis, yielding Bragg peaks and Bragg rods, respectively, are documented at three time points in Fig. 5. Illustrating first the control without lectin addition (a), data are then presented for the situation after 5 h ( $t_1$ ) and 13 h ( $t_2$ ), with approximately 14 and 20% area expansion of the lipid monolayer reached. The rate of area expansion due to lectin insertion was approximately 2%/h. Gal-1 insertion did not reach equilibrium after 13 h – a plateau in area/molecule vs. time was not observed.

The diffraction patterns obtained for the DPPE-GM1 monolayer at 20 mN/m and 20°C before and after applying Gal-1 enabled calculation of the set of structural parameters summarized in Tables 1 and 2.

For each of the systems measured, three Bragg peaks were observed, at  $q_{xy} \sim 1.42$ , 1.45, and  $1.48 \text{ \AA}^{-1}$ . The presence of three Bragg peaks is indicative of an oblique 2D cell. The integrated intensities of the three Bragg peaks ( $-0.05 \text{ \AA}^{-1} \leq q_z \leq 0.8 \text{ \AA}^{-1}$ ) were approximately the same (dashed lines in Fig. 5), in agreement with the multiplicity rule. The three peaks can be indexed as  $\{1,0\}$ ,  $\{0,1\}$  and  $\{1,-1\}$ . The calculated  $d$ -spacing values ( $d$ -spacing =

$2\pi/q_{xy}$ ), i.e.  $d_{10}$ ,  $d_{01}$ , and  $d_{1-1}$ , are attributed to a primitive 2D unit cell with dimensions of the unit vectors  $|\mathbf{a}|$ ,  $|\mathbf{b}|$ , the angle between them  $\gamma$ , and the area per two alkyl chains, which are all given in Table 1.

Assuming that the monolayer consists of perfect 2D crystallites of an average dimension  $L_{xy}$  (the lateral coherence length) in the crystallographic direction  $\{h, k\}$  with no preferred azimuthal orientation, the Scherrer formula [36] can be used to calculate the coherence length in the three crystallographic directions using the equation  $L_{xy} \approx 0.9 \cdot [2\pi/\text{FWHM}_{\text{intrinsic}}(q_{xy})] \{h, k\}$ . As the corresponding full width at half maximum (FWHM) of the three peaks exceeds the instrumental resolution of  $\text{FWHM}_{\text{resol}}(q_{xy}) = 0.0084 \text{ \AA}^{-1}$ , the intrinsic FWHM can be obtained using the equation  $\text{FWHM}_{\text{intrinsic}}(q_{xy}) = [\text{FWHM}_{\text{meas}}(q_{xy})^2 - \text{FWHM}_{\text{resol}}(q_{xy})^2]^{1/2}$ . From this analysis, the lateral coherence lengths for the three peaks,  $L_{10}$ ,  $L_{01}$ , and  $L_{1-1}$ , were estimated (Table 2). As a reference, a distance of 500 Å encompasses approximately 100 alkyl chains or a crystalline domain with 50 lipid units across.

The combined Bragg rod profile of the  $\{0,1\}$ ,  $\{1,0\}$ , and  $\{1,-1\}$  reflections, shown in Fig. 5 (a', b', c'), was produced by integrating the scattering data over the  $1.35 \text{ \AA}^{-1} \leq q_{xy} \leq 1.55 \text{ \AA}^{-1}$  region of the three peaks. The

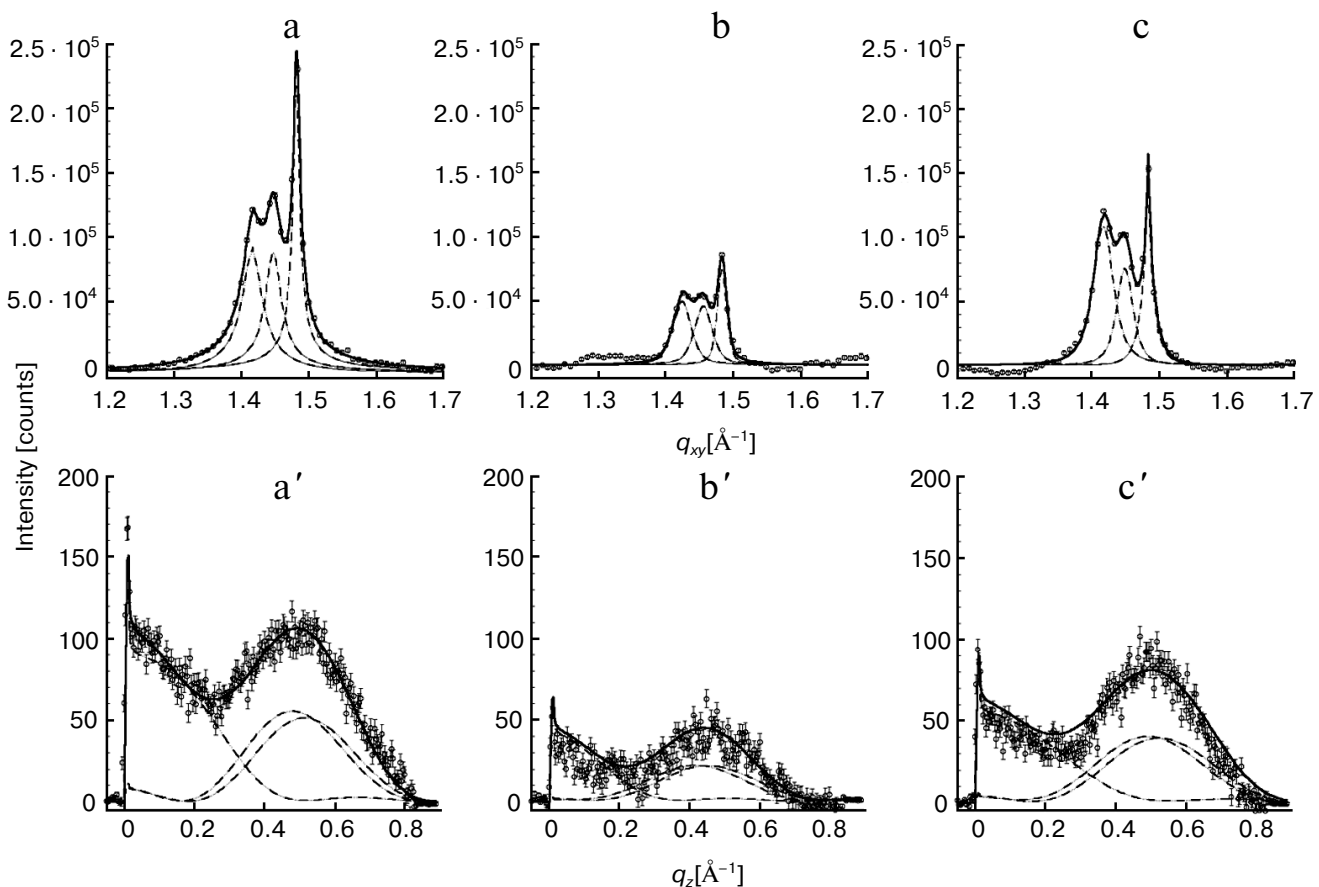


**Fig. 5.** Integrated GIXD (Bragg peaks) data of the lipid film before (a) and 5 h (b) and 13 h (c) after applying Gal-1. The diffraction pattern was fitted using the sum of three Voigt profiles (solid line) and deconvoluted into separate peaks (dashed lines) corresponding to each  $\{1,0\}$ ,  $\{0,1\}$  and  $\{1,-1\}$  Bragg peak. Bragg peaks were obtained by integrating over the  $(-0.05 \text{ \AA}^{-1} \leq q_x \leq 0.8 \text{ \AA}^{-1})$  region. a', b', c') Sum of the three  $\{1,0\}$ ,  $\{0,1\}$ ,  $\{1,-1\}$  Bragg rods corresponding to DPPE-GM1 and  $t_1 = 5 \text{ h}$  and  $t_2 = 13 \text{ h}$  after injection of Gal-1. By integrating over the  $(1.35 \text{ \AA}^{-1} \leq q_{xy} \leq 1.55 \text{ \AA}^{-1})$  region, the Bragg rods were fitted (solid line) by approximating the coherently scattering part of the alkyl tail by a cylinder of constant electron density. Each of the separate Bragg rods are shown as dashed lines.

Bragg rod profiles were analyzed by approximating the alkyl tails of the lipids as tilted cylinders with constant electron density and length  $L_c$  [33]. As expressed in the data given in Table 1 and illustrated in Fig. 5, the diffraction patterns from the DPPE-GM1 and DPPE-GM1 + Gal-1 ( $t_2 = 13 \text{ h}$ ) monolayers are similar, indicating that, in the ordered phase, they have a similar area per lipid molecule ( $43.5 \text{ \AA}^2$ ), alkyl tail tilt ( $\sim 21.45 \pm 0.15^\circ$  from the surface normal), and azimuthal angle ( $10.8 \pm 0.3^\circ$  from the nearest neighbor defined by the vector  $\mathbf{a} + \mathbf{b}$ ). However, the length of the cylinder with constant electron density used to model the intensity distribution along the Bragg rods,  $L_c$ , was  $18.9 \text{ \AA}$  for the galectin-free DPPE-GM1 monolayer vs.  $17.3 \text{ \AA}$  at  $t_2$ . This suggests that the exposure of the monolayer to Gal-1 caused a small ( $1.5 \text{ \AA}$ ) vertical displacement in lipid packing. Additionally, the  $L_{1-1}$  coherence length increased from  $500$  to  $760 \text{ \AA}$  at  $t_2$ , suggesting altered packing of the lipid tails along this crystallographic direction (Table 2).

The diffraction from the DPPE-GM1 + Gal-1 system at  $t_1$  (5 h) is different from the so far presented cases of pure lipids (no protein) or 13 h after lectin application. Although the length of the cylinder,  $L_c$ , was the same as in the case of the DPPE-GM1 monolayer before Gal-1 insertion ( $18.9 \text{ \AA}$ ), most likely excluding out-of-plane lipid displacements, the area per molecule decreased to  $43.1 \text{ \AA}^2$ , and alkyl tail tilt and azimuthal angle decreased to  $19.4$  and  $2.6^\circ$ , respectively. The  $L_{1-1}$  coherence length was also lowered from  $500$  to  $380 \text{ \AA}$ , suggesting a reduction in the positional registry between the lipid tails along this crystallographic direction (Table 2).

With the insertion of Gal-1, the intensity of the diffraction peaks decreased to about 35% at  $t_1$  compared to that of lipids alone, indicating that the crystalline order in lipid tails arrangement has been partially disrupted. Interestingly, this appeared as a transient phenomenon: partial recovery of relative quantity of ordered phase took place, because the integrated intensities increased to 70% at  $t_2 = 13 \text{ h}$ . Of note, such a course of parameter change

**Table 1.** Summary of parameters obtained from analysis of GIXD data

20 mN/m, 20°C	Primitive unit cell $a$ , $b$ , $\gamma$ (Å, Å, degrees)			Area per molecule (Å <sup>2</sup> )	Integ- rated inten- sity (%)	Coherence length, $L_c$ (Å)	Tilt angle, $t$ (°)	Tilt direction from NN, non-sym- metry (°)	$\sigma$ , Å
DPPE–GM1	$4.91 \pm 0.01$	$5.01 \pm 0.01$	$117.1 \pm 0.4$	$43.5 \pm 0.1$	100	$18.9 \pm 0.5$	$21.6 \pm 1.0$	$11.1 \pm 1.0$	$0.9 \pm 0.2$
DPPE–GM1 Gal-1, $t_1 = 5$ h	$4.89 \pm 0.01$	$5.00 \pm 0.01$	$118.0 \pm 0.4$	$43.1 \pm 0.1$	35	$18.9 \pm 0.5$	$19.4 \pm 1.0$	$2.6 \pm 2.0$	$0.94 \pm 0.2$
DPPE–GM1 Gal-1, $t_2 = 13$ h	$4.90 \pm 0.01$	$5.01 \pm 0.01$	$117.7 \pm 0.4$	$43.5 \pm 0.1$	70	$17.3 \pm 0.5$	$21.3 \pm 1.0$	$10.5 \pm 1.0$	$0.84 \pm 0.2$

Notes:  $L_c$  is the length of the coherently scattering part of the alkyl tail measured along its backbone. Tilt angle is measured from the surface normal. The tilt angle is measured between the direction of nearest neighbor and the projection of the alkyl tail on the subphase surface. Nearest neighbor (NN) is along  $\mathbf{a} + \mathbf{b}$ , where  $\mathbf{a}$  and  $\mathbf{b}$  are the 2D unit cell vectors;  $\sigma$  is the vertical Debye–Waller factor or root-mean-square molecular displacement normal to the surface.

has not been previously observed for any protein–membrane systems we have studied to date. Although the cause of this reestablishment of extent of the ordered phase is unclear, it is evident that the initial association of Gal-1 to the LC phase of the model lipid membrane was followed by reorganization and/or relaxation of the system such that the liquid-condensed phase reformed. Clustering and/or an *in situ* oligomerization of membrane-associated Gal-1 may, at least in part, underlie this process. The increase in the amount of the LC phase with incubation time could also be caused by large-scale heterogeneities, as would occur if lipid phase and protein were not uniformly distributed in the film. This is rather unlikely, because we have never observed such phenomena.

Interestingly, no diffraction signal was observed in the low  $q_{xy}$  region ( $0.05\text{--}1.0$  Å<sup>-1</sup>,  $120$  Å  $>$   $d$ -spacing  $>$   $6$  Å) corresponding with higher  $d$ -spacings of the measured spectra (data not shown). Therefore, we conclude that neither Gal-1 nor pentasaccharide headgroups of GM1 form regular arrays of sufficient size to be detectable by GIXD.

Whereas GIXD measurements probe the crystalline portion of the hydrocarbon chains in the footprint of the X-ray beam, XR provides averaged structural information from both the 2D-crystalline and the amorphous parts of the monolayer along the direction perpendicular to the lipid film. The reflectivity data were analyzed using an optical matrix method (StochFit) [37], assuming that the mixed monolayers establish thin homogeneous films. This is justified, because previous Brewster angle and fluorescent microscopy studies show that the components mix rather than phase separate [38–41]. Following the StochFit procedure [37], the electron density distribution, normalized to that of water, along the subphase surface normal was approximated by a large number of slabs, each with a constant electron density, interconnected by error functions. In this model-independent fitting procedure,

the electron density of each slab was varied to optimize a mathematical construct to obtain the smooth functional form of the electron density distribution, which results in the best fit (lowest  $\chi^2$  values) to the measured XR data. Twelve slabs were sufficient to adequately model XR profiles obtained from this study. The top row of Fig. 6 shows XR data (circles) along with the best fits (solid and dashed black lines) based on electron density distributions presented in the bottom row by solid gray lines.

As shown in Fig. 6, incorporation of the lectin induced substantial changes in the reflectivity profiles of the lipid monolayer (Fig. 6, a–c). Not surprisingly, electron density profiles from the model-independent fitting of XR data also appeared to undergo significant changes with insertion (solid gray profiles in Figs. 6a', 6b', and 6c'). To gain a better physical understanding of structural changes of the DPPE–GM1 monolayer upon contact with Gal-1, the electron density profiles obtained from the model-independent StochFit procedure were deconvoluted

**Table 2.** In-plane coherence lengths obtained from GIXD data

20 mN/m, 20°C	In-plane Bragg peak coherence length, $L_{xy}$ (Å) $\pm 10$ Å		
	$L_{01}$	$L_{10}$	$L_{1-1}$
DPPE–GM1	160	190	500
DPPE–GM1 + + Gal-1, $t_1 = 5$ h	180	180	380
DPPE–GM1 + + Gal-1, $t_2 = 13$ h	160	200	760

Note: Length,  $L_{xy}$ , is the in-plane coherence length; an average size of the 2D “crystalline” islands.

ed into three boxes (or slabs) of constant electron densities (dashed, step-like electron density distributions shown in bottom row of Fig. 6). This constitutes the model-dependent fitting of the XR data. Applying roughness (or smearing) to the step-like model-dependent profiles resulted in electron density distributions (solid black lines in the bottom row), almost indistinguishable from the original distribution of the model-independent fits (solid gray lines). The new electron density profiles can be used to calculate the XR (dashed lines, top row). These new fits, based on only three slabs, differ from model-independent fits exclusively at high momentum transfer vectors,  $q_z$ . Such a simple but physically reasonable model allows for a better understanding of the evolution of the system and provides a way to approximate spatial parameters of Gal-1 at the interface. As shown in Fig. 6a', and in agreement with previously published studies [38–41], the mixed DPPE–GM1 monolayer can be adequately modeled by three slabs: one for the GM1 headgroups and water, one for the mixed DPPE and GM1 headgroup region, and the third for the acyl tails of both (glyco)sphingolipids. The same scheme

of slabs was found to adequately model the XR data at both time points after the injection of Gal-1 into the subphase (Fig. 6, b' and c').

The following qualitative insight can be gained directly from the reflectivity profiles shown in Fig. 6: when the lectin was present in the subphase, the XR interference fringes became less distinguished. This is indicative of increased disorder (along surface normal) imposed on the perfectly aligned DPPE–GM1 monolayer by the presence of the lectin. Electron density profiles of the membrane before and after lectin insertion are overlaid and presented in Fig. 7a for direct comparison. It is immediately apparent that contact with Gal-1 molecules results in pronounced changes in the electron density distribution across the air/liquid interface. The initial three distinct slabs composed of tails/DPPE–GM1 headgroups/GM1 headgroups become less stratified, and more electrons are present towards the air interface after addition of Gal-1. Increasing incubation time and therefore extent of Gal-1 insertion resulted in a monotonic increase in the electron density in the lipid tail region (0 to 20 Å from the air inter-

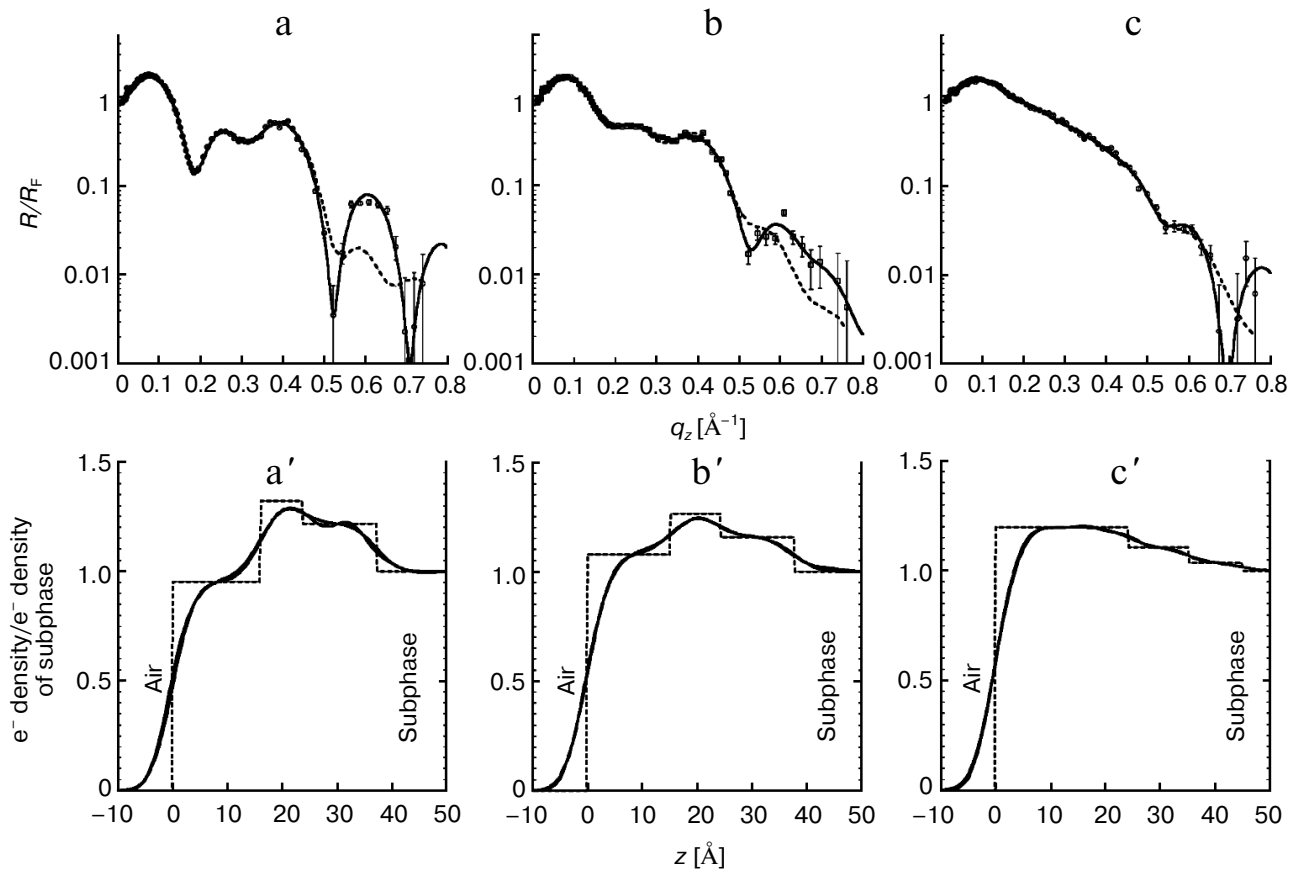


**Fig. 6.** Fresnel-normalized X-ray reflectivity (top row) and normalized electron density distribution (bottom row) of the DPPE–GM1 lipid films before (a and a') and at  $t_1 = 5$  h after Gal-1 injection (b, b') and  $t_2 = 13$  h after Gal-1 injection (c, c'). Measured data is represented as symbols, and lines (solid and dashed) represent fits corresponding to the electron density profiles shown in (a', b' and c'). The electron densities  $\rho(z)$  are normalized to the electron density of buffer subphase ( $\rho_{\text{subphase}} 0.335 \text{ e}^-/\text{\AA}^3$ ). Error bars for the reflectivity data represent statistical errors in these measurements.

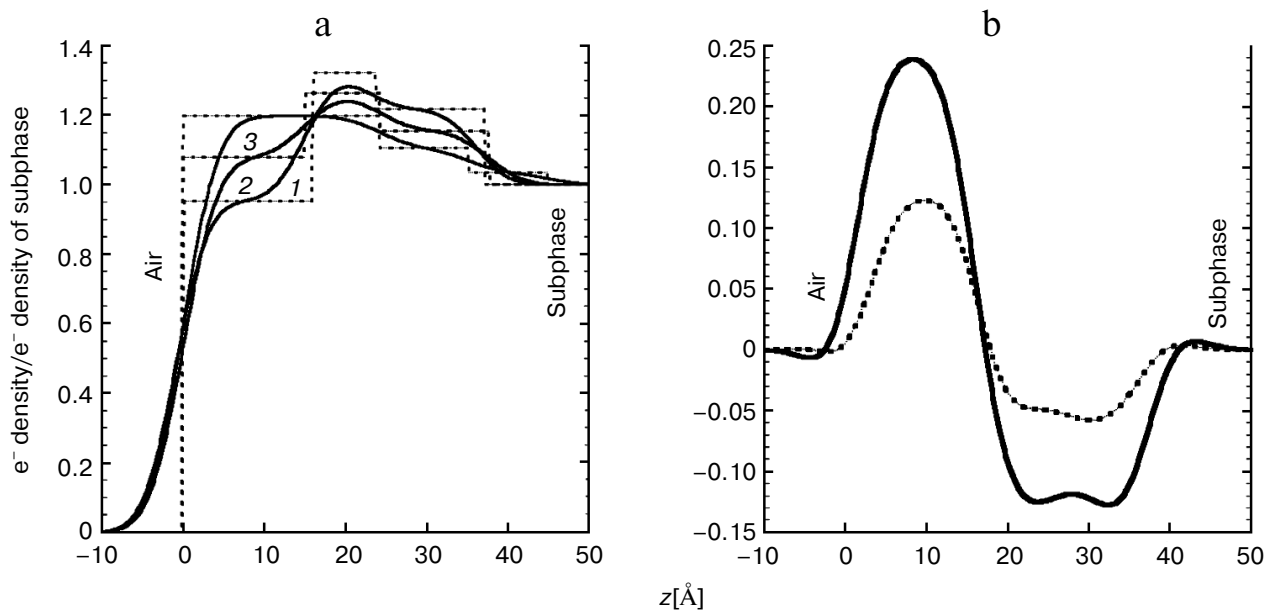


**Fig. 7.** a) Comparison of normalized electron density distribution for the DPPE–GM1 monolayer (1) and at  $t_1 = 5$  h (2) and  $t_2 = 13$  h (3) after Gal-1 injection. Dashed and solid lines represent the electron densities from the three-slab model that is unsmeared and smeared, respectively. The electron densities  $\rho(z)$  are normalized to the electron density of the liquid subphase ( $\rho_{\text{subphase}} = 0.335 \text{ e}^-/\text{\AA}^{-3}$ ). b) Differences between the electron density profiles of the DPPE–GM1 monolayer free of Gal-1 and the DPPE–GM1 lipid monolayers containing Gal-1 at  $t_1 = 5$  h (dashed line) and  $t_2 = 13$  h (solid line) after Gal-1 injection.

face) and decrease in the headgroup regions (approximately 20 to 40 Å towards the liquid subphase). These changes are more apparent when the differences between  $t_1$  and  $t_2$  electron density profiles and those of the lipids alone are calculated and plotted (Fig. 7b).

The integration of the area under the step-like profiles (dashed lines in Fig. 6, a'-c') provides information on the total number of electrons per  $\text{\AA}^2$  in the footprint of the X-ray beam. Despite the increase in the area per molecule (Fig. 3b) and therefore decrease in the number of DPPE–GM1 units, the number of electrons increased from  $14.0 \text{ e}^-/\text{\AA}^2$  for DPPE–GM1 to  $14.5$  and  $17.2 \text{ e}^-/\text{\AA}^2$  at  $t_1 = 5$  h and  $t_2 = 13$  h, respectively. These changes correspond to 4 and 23% increases in the number of electrons. Such enhancement can only be explained by the presence of lectin in the lipid monolayer. When corrected by the 14 and 20% increase in area per molecule due to lectin insertion, electron density increases were 19 and 48% at  $t_1$  and  $t_2$ , respectively. Therefore, at the final stage of the measurement ( $t = 13$  h), an approximately ~50% electron density increase can be attributed to the presence of Gal-1 in the monolayer.

## DISCUSSION

X-Ray scattering data of DPPE–GM1 monolayers at an air/buffer interface before and after injection of a multifunctional human lectin that is involved in modulat-

ing cellular activities including gene expression profiles [16, 42, 43] have been presented. We studied a 80 : 20 mol% DPPE/GM1 monolayer before and after injection of Gal-1-containing solution into the subphase at constant surface pressure of 20 mN/m and temperature of 20°C (final concentration of 21 µg/ml). Similar to previously published data [43], no phase separation of DPPE and GM1 components or lateral domain formation in these mixtures was detected. The GIXD results indicate that insertion of the lectin into the lipid monolayer affects the lipid-ordered (LC) phase of the monolayer, and this in a very peculiar manner. Upon contact with Gal-1, the packing arrangement of alkyl chains in the LC phase was only slightly changing. With time, after 5 h of incubation, the amount of the LC phase decreased to 35% of the original value, and then subsequently increased to 70% measured after 13 h of incubation (Table 1). The oblique 2D unit cell dimensions as well as size of the crystallite domains of the lectin-free DPPE–GM1 monolayer and at  $t_2 = 13$  h after Gal-1 injection to the buffer reservoir remained similar. Of note, for the intermediate time of  $t_1 = 5$  h, the changes in the packing of the alkyl tails (and overall intensity of the scattering) were very pronounced. An initial stage of strong molecular interplay may occur, after which the Gal-1 molecules may oligomerize, become more soluble, and leave the gel phase or, alternatively, acquire a different positioning vis-a-vis the ordered lipids leading to reconstitution of tail arrangements. The changes in the GIXD pattern indicate that Gal-1 mole-

cules have a tendency to interact with the ordered monolayer phase. The average distance between the lipid headgroups in the LC phase is approximately 10 Å (twice the value of the 2D cell dimensions; Table 1), and the average distance between GM1 headgroups for the 80 : 20 DPPE/GM1 mixture is ~30 Å. Therefore, it is expected that protein residues separated by such distances can influence these interactions.

The XR measurements show very substantial changes in the electron density distribution along the line perpendicular to the monolayer. Prior to injection of Gal-1-containing solution, the electron density distribution obtained from XR measurements shows that the DPPE headgroups and the proximal headgroups of ganglioside GM1 line up in the 2D monolayer plane. The branched portion of the pentasaccharide headgroup can extend further into the water subphase, minimizing lateral interactions. Modeling of GM1 conformations in an environment with phosphatidylcholine headgroups had inferred the potential for two constellations, referred to as “protruding” and “embedded” [44, 45]. The ganglioside sugar headgroup is easily detectable in the reflectivity profiles for  $t_0 = 0$  and  $t_1 = 5$  h.

Based on the measured electron density distributions (Fig. 7), there is clear evidence of Gal-1 penetration into the hydrophobic tail region of the lipid monolayer and/or staggering of the headgroups. The XR results indicate a significant increase in the number of electrons in the monolayer despite the increase in area per lipid molecule due to monolayer expansion. The excess of electrons can only be attributed to the presence of Gal-1 molecules at the interface. The resulting electron density distributions (Fig. 7, a and b) indicate that, along the direction of the surface normal, the length scale of ~40 Å is affected by the protein, corresponding to the short protein axis. Binding with the long axis parallel to the air/subphase interface is thus likely. There is also clear evidence that insertion of the Gal-1 influences the hydrophobic (alkyl tail) region of the monolayer. Despite a strong impact on electron density distribution of the DPPE–GM1 monolayer by contact with Gal-1, no clear evidence of location of the molecules in a regular stratum below the monolayer was observed. The low  $q_{xy}$  GIXD studies did not detect any in-plane ordered structures of  $d$ -spacings shorter than 120 Å. These data are in line with the reasoning that no in-plane ordering of Gal-1 into regular 2D arrays occurred. Interplay of Gal-1 and the DPPE–GM1 monolayer is dependent on the surface pressure. Of note, at 30 mN/m we observed no protein insertion into the monolayer.

Contrary to the XR results, the GIXD obtained after 13 h of Gal-1 incubation showed only small changes in the gel phase of the monolayer. Thus, we can deduce that the protein molecules are predominantly in contact with the liquid-expanded phase. This is also supported by the fact that at higher surface pressures (when the amount of

the ordered phase is increasing) no evidence of insertion was observed.

In comparison to previous work with Ctx, the mode of interplay of the 80 : 20 DPPE/GM1 monolayer with Gal-1 is different from that of Ctx ( $B_5$  and  $AB_5$ ) [38–40]. Ctx (gently) attached to the monolayer from the bottom altering the in-plane and out-of-plane structure of the monolayer (alkyl tails) to a much lesser extent than Gal-1. At the initial stages of interactions, Ctx formed a rather homogeneous monolayer below the headgroups of PE–GM1. Additionally, Ctx molecules organized themselves in 2D crystallites with high degree of in-plane coherency. Nothing like that was observed for Gal-1. Elongated homodimeric Gal-1 (ellipsoid with the two principal lengths of approximately 40 and 56 Å; sedimentation-velocity data yielded a friction ratio of approximately 1.3 [46]) with separation of the two lectin sites by approximately 40–45 Å and their characteristic orientation (almost parallel to the long axis of the molecule [47]) cause a significant disruption in the order of the alkyl tails of monolayer, as schematically indicated in Fig. 2c. For the 80 : 20 DPPE/GM1 mixture, on average along one dimension, the GM1 headgroups are separated by a distance of 30 Å. Incommensurability of the distances (separation of Gal-1 binding sites and the averaged distance between the GM1 headgroups) leads to increased level of disorder for the alkyl tail packing when both binding sites are engaged. Overall, the presented results thus illustrate that the two receptor types affect membrane properties to different extents.

In addition to the specific glycan–lectin interaction, the possibility should be considered that the carbohydrate recognition domain of galectins could be capable of engaging in a lipid–monolayer contact, as e.g. known from annexins [48, 49]. Previous work on Gal-3 found the lectin to interact with phosphatidylserine, galactosylceramide, and cholesterol and to rapidly penetrate and traverse a lipid bilayer (molar ratio of 2.1 : 5.0 : 0.1 of cholesterol, dimyristoyl-L- $\alpha$ -phosphatidylcholine, and dicetyl phosphate) [50], yet left open the possibility that the tail region with the collagen-like repeats and N-terminal peptide of the chimera-type galectin could be responsible for this property.

Because galectins are synthesized on free cytoplasmic ribosomes and secreted by unconventional pathway(s) [51, 52] and ganglioside GM1 is also a constituent of nuclear membranes [53, 54], these data may have further relevance for understanding secretion and intracellular trafficking, Gal-1 having been localized in cell nuclei [55–58]. With the topological presentation of binding sites, reactivity to glycoclusters/cell surfaces and the functional consequences of binding being different among galectins [16, 23, 59–67], even antagonistic in certain cases [12, 68], and rational engineering capable of providing variants for deliberate probing of structure–activity properties [66, 69], systematic application of this

method is warranted to delineate glycan structure–lectin binding profiles. Of note, galectins are present as a network *in vivo*, with the possibility for functional competition [7, 70]. Moving on to a model bilayer [71] and adding cholesterol will help increase the level of biorelevance. However, the steroid had been reported to reduce glycan accessibility by tilting the sugar chain of glycosphingolipids toward the membrane phase and to form a compositional asymmetry with GM1 [72–74]. Consequently, unmasking of previously “invisible” glycosphingolipid was possible by cholesterol extraction, e.g. using methyl- $\beta$ -cyclodextrin [73, 75]. Doing so for neuroblastoma (SK-N-MC) cells decreased the  $B_{\max}$  value for binding of Gal-1 from about 300 to nearly 170 fmol, with a nearly 10-fold increase in dissociation constant [14]. In parallel, surface binding and its relevance for *trans*-interactions can be evaluated using custom-made glycodynamersomes (vesicles of defined size obtained by self-assembly of amphiphilic Janus glycodynamers) in aggregation assays [76–79], complementing the analysis of structural aspects in *cis*-constellations. These experimental lines will contribute to crack the sugar code [80–82], in the topological context of biorelevant surfaces.

The Los Alamos Neutron Science Center at the Los Alamos National Laboratory is funded by the US Department of Energy under contract W-7405-ENG-36. EYC and EJ would like to acknowledge funding from Oakridge Associated Universities Ralph E. Powe Junior Faculty Enhancement Award and the University of New Mexico Research Allocation Committee for supporting the X-ray scattering experiments. We would also like to acknowledge EC funding (GLYCOPHARM, contract No. 317297), HASYLAB for beam time, Dr. B. Struth for help with the reflectivity and grazing incidence diffraction experiments, and Drs. J. Domingo-Ekark and B. Friday for inspiring discussions.

## REFERENCES

- Kopitz, J. (2009) in *The Sugar Code. Fundamentals of Glycosciences* (Gabius, H.-J., ed.) Wiley-VCH, Weinheim, pp. 177–198.
- Ledeen, R. W., and Wu, G. (2009) in *The Sugar Code. Fundamentals of Glycosciences* (Gabius, H.-J., ed.) Wiley-VCH, Weinheim, pp. 495–516.
- Wennekes, T., van den Berg, R. J., Boot, R. G., van der Marel, G. A., Overkleeft, H. S., and Aerts, J. M. (2009) Glycosphingolipids: nature, function, and pharmacological modulation, *Angew. Chem. Int. Ed.*, **48**, 848–869.
- Pontier, S. M., and Schweigert, F. (2012) Glycosphingolipids in signaling and development: from liposomes to model organisms, *Dev. Dyn.*, **241**, 92–106.
- Gabius, H.-J. (2001) Probing the cons and pros of lectin-induced immunomodulation: case studies for the mistletoe lectin and galectin-1, *Biochimie*, **83**, 659–666.
- Rapoport, E. M., Kurmyshkina, O. V., and Bovin, N. V. (2008) Mammalian galectins: structure, carbohydrate specificity, and functions, *Biochemistry (Moscow)*, **73**, 393–405.
- Kaltner, H., and Gabius, H.-J. (2012) A toolbox of lectins for translating the sugar code: the galectin network in phylogenesis and tumors, *Histol. Histopathol.*, **27**, 397–416.
- Solis, D., Bovin, N. V., Davis, A. P., Jimenez-Barbero, J., Romero, A., Roy, R., Smetana, K., Jr., and Gabius, H.-J. (2015) A guide into glycosciences: how chemistry, biochemistry and biology cooperate to crack the sugar code, *Biochim. Biophys. Acta*, **1850**, 186–235.
- Siebert, H.-C., Andre, S., Lu, S.-Y., Frank, M., Kaltner, H., van Kuik, J. A., Korchagina, E. Y., Bovin, N. V., Tajkhorshid, E., Kaptein, R., Vliegenthart, J. F. G., von der Lieth, C.-W., Jimenez-Barbero, J., Kopitz, J., and Gabius, H.-J. (2003) Unique conformer selection of human growth-regulatory lectin galectin-1 for ganglioside GM1 versus bacterial toxins, *Biochemistry*, **42**, 14762–14773.
- Andre, S., Kaltner, H., Lensch, M., Russwurm, R., Siebert, H.-C., Fallsehr, C., Tajkhorshid, E., Heck, A. J. R., von Knebel Doeberitz, M., Gabius, H.-J., and Kopitz, J. (2005) Determination of structural and functional overlap/divergence of five proto-type galectins by analysis of the growth-regulatory interaction with ganglioside GM1 *in silico* and *in vitro* on human neuroblastoma cells, *Int. J. Cancer*, **114**, 46–57.
- Dettmann, W., Grandbois, M., Andre, S., Benoit, M., Wöhle, A. K., Kaltner, H., Gabius, H.-J., and Gaub, H. E. (2000) Differences in zero-force and force-driven kinetics of ligand dissociation from  $\beta$ -galactoside-specific proteins (plant and animal lectins, immunoglobulin G) monitored by plasmon resonance and dynamic single molecule force microscopy, *Arch. Biochem. Biophys.*, **383**, 157–170.
- Kopitz, J., von Reitzenstein, C., Andre, S., Kaltner, H., Uhl, J., Ehmann, V., Cantz, M., and Gabius, H.-J. (2001) Negative regulation of neuroblastoma cell growth by carbohydrate-dependent surface binding of galectin-1 and functional divergence from galectin-3, *J. Biol. Chem.*, **276**, 35917–35923.
- Wang, J., Lu, Z.-H., Gabius, H.-J., Rohowsky-Kochan, C., Ledeen, R. W., and Wu, G. (2009) Cross-linking of GM1 ganglioside by galectin-1 mediates regulatory T cell activity involving TRPC5 channel activation: possible role in suppressing experimental autoimmune encephalomyelitis, *J. Immunol.*, **182**, 4036–4045.
- Kopitz, J., Bergmann, M., and Gabius, H.-J. (2010) How adhesion/growth-regulatory galectins-1 and -3 attain cell specificity: case study defining their target on neuroblastoma cells (SK-N-MC) and marked affinity regulation by affecting microdomain organization of the membrane, *IUBMB Life*, **62**, 624–628.
- Wu, G., Lu, Z.-H., Gabius, H.-J., Ledeen, R. W., and Bleich, D. (2011) Ganglioside GM1 deficiency in effector T cells from NOD mice induces resistance to regulatory T-cell suppression, *Diabetes*, **60**, 2341–2349.
- Ledeen, R. W., Wu, G., Andre, S., Bleich, D., Huet, G., Kaltner, H., Kopitz, J., and Gabius, H.-J. (2012) Beyond glycoproteins as galectin counter-receptors: tumor/effector T cell growth control via ganglioside GM1, *Ann. N. Y. Acad. Sci.*, **1253**, 206–221.

17. Lencer, W. I., and Saslowsky, D. (2005) Raft trafficking of AB<sub>5</sub> subunit bacterial toxins, *Biochim. Biophys. Acta*, **1746**, 314-321.
18. Beddoe, T., Paton, A. W., Le Nours, J., Rossjohn, J., and Paton, J. C. (2010) Structure, biological functions and applications of the AB<sub>5</sub> toxins, *Trends Biochem. Sci.*, **35**, 411-418.
19. Fajka-Boja, R., Blasko, A., Kovacs-Solyom, F., Szelenyi, G. J., Toth, G. K., and Monostori, E. (2008) Co-localization of galectin-1 with GM1 ganglioside in the course of its clathrin- and raft-dependent endocytosis, *Cell. Mol. Life Sci.*, **65**, 2586-2593.
20. Sobel, D. O., Yankelevich, B., Goyal, D., Nelson, D., and Mazumder, A. (1998) The B-subunit of cholera toxin induces immunoregulatory cells and prevents diabetes in the NOD mouse, *Diabetes*, **47**, 186-191.
21. Williams, N. A., Hirst, T. R., and Nashar, T. O. (1999) Immune modulation by the cholera-like enterotoxins: from adjuvant to therapeutic, *Immunol. Today*, **20**, 95-101.
22. Salmond, R. J., Luross, J. A., and Williams, N. A. (2002) Immune modulation by the cholera-like enterotoxins, *Expert Rev. Mol. Med.*, **4**, 1-16.
23. Kopitz, J., Ballikaya, S., Andre, S., and Gabius, H.-J. (2012) Ganglioside GM1/galectin-dependent growth regulation in human neuroblastoma cells: special properties of bivalent galectin-4 and significance of linker length for ligand selection, *Neurochem. Res.*, **37**, 1267-1276.
24. Gupta, R. K., Pande, A. H., Gulla, K. C., Gabius, H.-J., and Hajela, K. (2006) Carbohydrate-induced modulation of cell membrane. VIII. Agglutination with mammalian lectin galectin-1 increases osmofragility and membrane fluidity of trypsinized erythrocytes, *FEBS Lett.*, **580**, 1691-1695.
25. He, L., Andre, S., Siebert, H.-C., Helmholz, H., Niemeyer, B., and Gabius, H.-J. (2003) Detection of ligand- and solvent-induced shape alterations of cell-growth-regulatory human lectin galectin-1 in solution by small angle neutron and X-ray scattering, *Biophys. J.*, **85**, 511-524.
26. Purkrabkova, T., Smetana, K., Jr., Dvorankova, B., Holikova, Z., Bock, C., Lensch, M., Andre, S., Pytlik, R., Liu, F.-T., Klima, J., Smetana, K., Motlik, J., and Gabius, H.-J. (2003) New aspects of galectin functionality in nuclei of cultured bone marrow stromal and epidermal cells: biotinylated galectins as tool to detect specific binding sites, *Biol. Cell*, **95**, 535-545.
27. Andre, S., Sanchez-Ruderisch, H., Nakagawa, H., Buchholz, M., Kopitz, J., Forberich, P., Kemmner, W., Bock, C., Deguchi, K., Detjen, K. M., Wiedenmann, B., von Knebel Doeberitz, M., Gress, T. M., Nishimura, S.-I., Rosewicz, S., and Gabius, H.-J. (2007) Tumor suppressor p16<sup>INK4a</sup>: modulator of glycomic profile and galectin-1 expression to increase susceptibility to carbohydrate-dependent induction of anoikis in pancreatic carcinoma cells, *FEBS J.*, **274**, 3233-3256.
28. Amano, M., Eriksson, H., Manning, J. C., Detjen, K. M., Andre, S., Nishimura, S.-I., Lehtio, J., and Gabius, H.-J. (2012) Tumor suppressor p16<sup>INK4a</sup>: anoikis-favoring decrease in N/O-glycan/cell surface sialylation by down-regulation of enzymes in sialic acid biosynthesis in tandem in a pancreatic carcinoma model, *FEBS J.*, **279**, 4062-4080.
29. Majewski, J., Popovitz-Biro, R., Bouwman, W. G., Kjaer, K., Als-Nielsen, J., Lahav, M., and Leiserowitz, L. (1995) The structural properties of uncompressed crystalline monolayers of alcohols C<sub>n</sub>H<sub>2n</sub>+1OH (n = 13-31) on water and their role as ice nucleators, *Chem. Eur. J.*, **1**, 304-311.
30. Als-Nielsen, J., and Kjær, K. (1999) in *Phase Transitions in Soft Condensed Matter* (Riste, T., and Sherrington, D., eds.) Springer, pp. 113-138.
31. Kjær, K. (1994) Some simple ideas on X-ray reflection and grazing-incidence diffraction from thin surfactant films, *Physica B: Condensed Matter*, **198**, 100-109.
32. Eisenberger, P., and Marra, W. C. (1981) X-Ray diffraction study of the Ge(001) reconstructed surface, *Phys. Rev. Lett.*, **46**, 1081-1084.
33. Als-Nielsen, J., Jacquemain, D., Kjaer, K., Leveiller, F., Lahav, M., and Leiserowitz, L. (1994) Principles and applications of grazing incidence X-ray and neutron scattering from ordered molecular monolayers at the air-water interface, *Phys. Rep.*, **246**, 251-313.
34. Jensen, T. R., Balashev, K., Bjornholm, T., and Kjaer, K. (2001) Novel methods for studying lipids and lipases and their mutual interaction at interfaces. Part II. Surface sensitive synchrotron X-ray scattering, *Biochimie*, **83**, 399-408.
35. Seelig, A. (1987) Local anesthetics and pressure: a comparison of dibucaine binding to lipid monolayers and bilayers, *Biochim. Biophys. Acta*, **899**, 196-204.
36. Guinier, A. (1963) *X-Ray Diffraction in Crystals, Imperfect Crystals, and Amorphous Bodies*, W. H. Freeman, San Francisco.
37. Danauskas, S. M., Li, D., Meron, M., Lin, B., and Lee, K. Y. C. (2008) Stochastic fitting of specular X-ray reflectivity data using StochFit, *J. Appl. Crystallogr.*, **41**, 1187-1193.
38. Miller, C. E., Majewski, J., Watkins, E. B., and Kuhl, T. L. (2008) An X-ray scattering study of cholera toxin penetration and induced phase transformations in lipid membranes, *Biophys. J.*, **95**, 629-640.
39. Miller, C. E., Majewski, J., Watkins, E. B., Weygand, M., and Kuhl, T. L. (2008) Diffraction from two-dimensional cholera toxin crystals bound to their receptors in a lipid monolayer, *Biophys. J.*, **95**, 641-647.
40. Watkins, E. B., Miller, C. E., Majewski, J., and Kuhl, T. L. (2011) Membrane texture induced by specific protein binding and receptor clustering: active roles for lipids in cellular function, *Proc. Natl. Acad. Sci. USA*, **108**, 6975-6980.
41. Majewski, J., Kuhl, T. L., Kjaer, K., and Smith, G. S. (2001) Packing of ganglioside-phospholipid monolayers: an X-ray diffraction and reflectivity study, *Biophys. J.*, **81**, 2707-2715.
42. Smetana, K., Jr., Andre, S., Kaltner, H., Kopitz, J., and Gabius, H.-J. (2013) Context-dependent multifunctionality of galectin-1: a challenge for defining the lectin as therapeutic target, *Expert Opin. Ther. Targets*, **17**, 379-392.
43. Martinez-Bosch, N., Fernandez-Barrena, M. G., Moreno, M., Ortiz-Zapater, E., Munne-Collado, J., Iglesias, M., Andre, S., Gabius, H.-J., Hwang, R. F., Poirier, F., Navas, C., Guerra, C., Fernandez-Zapico, M. E., and Navarro, P. (2014) Galectin-1 drives pancreatic carcinogenesis through stroma remodeling and hedgehog signaling activation, *Cancer Res.*, **74**, 3512-3524.
44. Patel, R. Y., and Balaji, P. V. (2007) Characterization of the conformational and orientational dynamics of ganglioside GM1 in a dipalmitoylphosphatidylcholine bilayer by

- molecular dynamics simulations, *Biochim. Biophys. Acta*, **1768**, 1628–1640.
45. Jedlovszky, P., Sega, M., and Vallauri, R. (2009) GM1 ganglioside embedded in a hydrated DOPC membrane: a molecular dynamics simulation study, *J. Phys. Chem. B*, **113**, 4876–4886.
  46. Kaltner, H., Solis, D., Kopitz, J., Lensch, M., Lohr, M., Manning, J. C., Mürnseer, M., Schnolzer, M., Andre, S., Saiz, J. L., and Gabius, H.-J. (2008) Prototype chicken galectins revisited: characterization of a third protein with distinctive hydrodynamic behaviour and expression pattern in organs of adult animals, *Biochem. J.*, **409**, 591–599.
  47. Lopez-Lucendo, M. F., Solis, D., Andre, S., Hirabayashi, J., Kasai, K.-I., Kaltner, H., Gabius, H.-J., and Romero, A. (2004) Growth-regulatory human galectin-1: crystallographic characterisation of the structural changes induced by single-site mutations and their impact on the thermodynamics of ligand binding, *J. Mol. Biol.*, **343**, 957–970.
  48. Zeng, F.-Y., Gerke, V., and Gabius, H.-J. (1993) Identification of annexin II, annexin VI and glyceraldehyde-3-phosphate dehydrogenase as calcyclin-binding proteins in bovine heart, *Int. J. Biochem.*, **25**, 1019–1027.
  49. Gerke, V., and Moss, S. E. (2002) Annexins: from structure to function, *Physiol. Rev.*, **82**, 331–371.
  50. Lukyanov, P., Furtak, V., and Ochieng, J. (2005) Galectin-3 interacts with membrane lipids and penetrates the lipid bilayer, *Biochem. Biophys. Res. Commun.*, **338**, 1031–1036.
  51. Wilson, T. J. G., Firth, M. N., Powell, J. T., and Harrison, F. L. (1989) The sequence of the mouse 14 kDa  $\beta$ -galactoside-binding lectin and evidence for its synthesis on free cytoplasmic ribosomes, *Biochem. J.*, **261**, 847–852.
  52. Hughes, R. C. (1999) Secretion of the galectin family of mammalian carbohydrate-binding proteins, *Biochim. Biophys. Acta*, **1473**, 172–185.
  53. Ledeen, R. W., and Wu, G. (2006) Sphingolipids of the nucleus and their role in nuclear signaling, *Biochim. Biophys. Acta*, **1761**, 588–598.
  54. Ledeen, R., and Wu, G. (2011) New findings on nuclear gangliosides: overview on metabolism and function, *J. Neurochem.*, **116**, 714–720.
  55. Saussez, S., Decaestecker, C., Lorfèvre, F., Chevalier, D., Mortuaire, G., Kaltner, H., Andre, S., Toubeau, G., Gabius, H.-J., and Leroy, X. (2008) Increased expression and altered intracellular distribution of adhesion/growth-regulatory lectins galectins-1 and during tumour progression in hypopharyngeal and laryngeal squamous cell carcinomas, *Histopathology*, **52**, 483–493.
  56. Nasrabadi, D., Larijani, M. R., Fathi, A., Gourabi, H., Dizaj, A. V., Baharvand, H., and Salekdeh, G. H. (2010) Nuclear proteome analysis of monkey embryonic stem cells during differentiation, *Stem Cell Rev.*, **6**, 50–61.
  57. Kodet, O., Dvorankova, B., Lacina, L., Andre, S., Kaltner, H., Gabius, H.-J., and Smetana, K., Jr. (2011) Comparative analysis of the nuclear presence of adhesion/growth-regulatory galectins and reactivity in the nuclei of interphasic and mitotic cells, *Folia Biol.*, **57**, 125–132.
  58. Remmeliink, M., de Leval, L., Decaestecker, C., Duray, A., Crompton, E., Sirtaine, N., Andre, S., Kaltner, H., Leroy, X., Gabius, H.-J., and Saussez, S. (2011) Quantitative immunohistochemical fingerprinting of adhesion/growth-regulatory galectins in salivary gland tumours: divergent profiles with diagnostic potential, *Histopathology*, **58**, 543–556.
  59. Villalobo, A., Nogales-Gonzalez, A., and Gabius, H.-J. (2006) A guide to signaling pathways connecting protein–glycan interaction with the emerging versatile effector functionality of mammalian lectins, *Trends Glycosci. Glycotechnol.*, **99**, 1–37.
  60. Rapoport, E. M., Andre, S., Kurmyshkina, O. V., Pochechueva, T. V., Severov, V. V., Pazynina, G. V., Gabius, H.-J., and Bovin, N. V. (2008) Galectin-loaded cells as a platform for the profiling of lectin specificity by fluorescent neoglycoconjugates: a case study on galectins-1 and -3 and the impact of assay setting, *Glycobiology*, **18**, 315–324.
  61. Chernyy, E. S., Rapoport, E. M., Andre, S., Kaltner, H., Gabius, H.-J., and Bovin, N. V. (2011) Galectins promote the interaction of influenza virus with its target cell, *Biochemistry (Moscow)*, **76**, 958–967.
  62. Dvorankova, B., Szabo, P., Lacina, L., Gal, P., Uhrova, J., Zima, T., Kaltner, H., Andre, S., Gabius, H.-J., Sykova, E., and Smetana, K., Jr. (2011) Human galectins induce conversion of dermal fibroblasts into myofibroblasts and production of extracellular matrix: potential application in tissue engineering and wound repair, *Cells Tissues Organs*, **194**, 469–480.
  63. Vokhmyanina, O. A., Rapoport, E. M., Ryzhov, I. M., Korchagina, E. Y., Pazynina, G. V., Severov, V. V., Kaltner, H., Andre, S., Gabius, H.-J., and Bovin, N. V. (2011) Carbohydrate specificity of chicken and human tandem-repeat-type galectins-8 in composition of cells, *Biochemistry (Moscow)*, **76**, 1185–1192.
  64. Vokhmyanina, O. A., Rapoport, E. M., Andre, S., Severov, V. V., Ryzhov, I., Pazynina, G. V., Korchagina, E., Gabius, H.-J., and Bovin, N. V. (2012) Comparative study of the glycan specificities of cell-bound human tandem-repeat-type galectins-4, -8 and -9, *Glycobiology*, **22**, 1207–1217.
  65. Murphy, P. V., Andre, S., and Gabius, H.-J. (2013) The third dimension of reading the sugar code by lectins: design of glycoclusters with cyclic scaffolds as tools with the aim to define correlations between spatial presentation and activity, *Molecules*, **18**, 4026–4053.
  66. Andre, S., Wang, G. N., Gabius, H.-J., and Murphy, P. V. (2014) Combining glycocluster synthesis with protein engineering: an approach to probe into the significance of linker length in a tandem-repeat-type lectin (galectin-4), *Carbohydr. Res.*, **389**, 25–38.
  67. Ruiz, F. M., Scholz, B. A., Buzamet, E., Kopitz, J., Andre, S., Menendez, M., Romero, A., Solis, D., and Gabius, H.-J. (2014) Natural single amino acid polymorphism (F19Y) in human galectin-8: detection of structural alterations and increased growth-regulatory activity on tumor cells, *FEBS J.*, **281**, 1446–1464.
  68. Sanchez-Ruderisch, H., Fischer, C., Detjen, K. M., Welzel, M., Wimmel, A., Manning, J. C., Andre, S., and Gabius, H.-J. (2010) Tumor suppressor p16<sup>INK4a</sup>: downregulation of galectin-3, an endogenous competitor of the pro-apoptotic effector galectin-1, in a pancreatic carcinoma model, *FEBS J.*, **277**, 3552–3563.
  69. Kopitz, J., Vertes, S., Andre, S., Fiedler, S., Schnolzer, M., and Gabius, H.-J. (2014) Human chimera-type galectin-3: defining the critical tail length for high-affinity glycoprotein/cell surface binding and functional competition with galectin-1 in neuroblastoma cell growth regulation, *Biochimie*, **104**, 90–99.

70. Dawson, H., Andre, S., Karamitopoulou, E., Zlobec, I., and Gabius, H.-J. (2013) The growing galectin network in colon cancer and clinical relevance of cytoplasmic galectin-3 reactivity, *Anticancer Res.*, **33**, 3053-3059.
71. Jose, B., Mallon, C. T., Forster, R. J., Blackledge, C., and Keyes, T. E. (2011) Lipid bilayer assembly at a gold nanocavity array, *Chem. Commun.*, **47**, 12530-12532.
72. Mahfoud, R., Manis, A., Binnington, B., Ackerley, C., and Lingwood, C. A. (2010) A major fraction of glycosphingolipids in model and cellular cholesterol-containing membranes is undetectable by their binding proteins, *J. Biol. Chem.*, **285**, 36049-36059.
73. Lingwood, D., Binnington, B., Rog, T., Vattulainen, I., Grzybek, M., Coskun, U., Lingwood, C. A., and Simons, K. (2011) Cholesterol modulates glycolipid conformation and receptor activity, *Nat. Chem. Biol.*, **7**, 260-262.
74. Rondelli, V., Fragneto, G., Motta, S., Del Favero, E., Brocca, P., Sonnino, S., and Cantu, L. (2012) Ganglioside GM1 forces the redistribution of cholesterol in a biomimetic membrane, *Biochim. Biophys. Acta*, **1818**, 2860-2867.
75. Novak, A., Binnington, B., Ngan, B., Chadwick, K., Fleshner, N., and Lingwood, C. A. (2013) Cholesterol masks membrane glycosphingolipid tumor-associated antigens to reduce their immunodetection in human cancer biopsies, *Glycobiology*, **23**, 1230-1239.
76. Percec, V., Leowanawat, P., Sun, H. J., Kulikov, O., Nusbaum, C. D., Tran, T. M., Bertin, A., Wilson, D. A., Peterca, M., Zhang, S., Kamat, N. P., Vargo, K., Moock, D., Johnston, E. D., Hammer, D. A., Pochan, D. J., Chen, Y., Chabre, Y. M., Shiao, T. C., Bergeron-Brlek, M., Andre, S., Roy, R., Gabius, H.-J., and Heiney, P. A. (2013) Modular synthesis of amphiphilic Janus glycodendrimers and their self-assembly into glycodendrimersomes and other complex architectures with bioactivity to biomedically relevant lectins, *J. Am. Chem. Soc.*, **135**, 9055-9077.
77. Zhang, S., Moussodia, R. O., Sun, H. J., Leowanawat, P., Muncan, A., Nusbaum, C. D., Chelling, K. M., Heiney, P. A., Klein, M. L., Andre, S., Roy, R., Gabius, H.-J., and Percec, V. (2014) Mimicking biological membranes with programmable glycan ligands self-assembled from amphiphilic Janus glycodendrimers, *Angew. Chem. Int. Ed.*, **53**, 10899-10903.
78. Zhang, S., Moussodia, R. O., Murzeau, C., Sun, H. J., Klein, M. L., Vertesy, S., Andre, S., Roy, R., Gabius, H.-J., and Percec, V. (2015) Dissecting molecular aspects of cell interactions using glycodendrimersomes with programmable glycan presentation and engineered human lectins, *Angew. Chem. Int. Ed.*, **54**, 4036-4040.
79. Zhang, S., Moussodia, R. O., Vertesy, S., André, S., Klein, M. L., Gabius, H.-J., and Percec, V. (2015) Unraveling functional significance of natural variations of a human galectin by glycodendrimersomes with programmable glycan surface, *Proc. Natl. Acad. Sci. USA*, **112**, 5585-5590.
80. Gabius, H.-J. (2015) The magic of the sugar code, *Trends Biochem. Sci.*, **40**, 341.
81. Gabius, H.-J., Kaltner, H., Kopitz, J., and André, S. (2015) The glycobiology of the CD system: a dictionary for translating marker designations into glycan/lectin structure and function, *Trends Biochem. Sci.*, **40**, 360-376.
82. Ledeen, R. W., and Wu, G. (2015) The multi-tasked life of GM1 ganglioside: a true factotum of nature, *Trends Biochem. Sci.*, **40**, 407-418.